Radiology

Thin-Section CT of the Secondary Pulmonary Lobule: Anatomy and the Image—The 2004 Fleischner Lecture[1]

W. Richard Webb, MD

The secondary pulmonary lobule is a fundamental unit of lung structure, and it reproduces the lung in miniature. Airways, pulmonary arteries, veins, lymphatics, and the lung interstitium are all represented at the level of the secondary lobule. Several of these components of the secondary lobule are normally visible on thin-section computed tomographic (CT) scans of the lung. The recognition of lung abnormalities relative to the structures of the secondary lobule is fundamental to the interpretation of thin-section CT scans. Pathologic alterations in secondary lobular anatomy visible on thin-section CT scans include interlobular septal thickening and diseases with peripheral lobular distribution, centrilobular abnormalities, and panlobular abnormalities. The differential diagnosis of lobular abnormalities is based on comparisons between lobular anatomy and lung pathology.

[1] From the Department of Radiology, University of California San Francisco, 505 Parnassus Ave, San Francisco, CA 94143-0628. Received November 19, 2004; revision requested January 10, 2005; revision received February 16; accepted March 9; final review by the author March 18. **Address correspondence to** the author (e-mail: *rwebb@radiology.ucsf.edu*).

Radiology

The secondary pulmonary lobule is a fundamental unit of lung structure, and an understanding of lobular anatomy is essential to the interpretation of thin-section computed tomographic (CT) scans of the lung. Thin-section CT can show many features of the secondary pulmonary lobule in both normal and abnormal lungs, and many lung diseases produce characteristic abnormalities of lobular anatomy (1–7).

The Secondary Pulmonary Lobule and Lung Acinus

The lung is made up of numerous anatomic units smaller than a lobe or segment. The secondary pulmonary lobule and lung acinus are widely regarded to be the most important of these subsegmental lung units.

The secondary pulmonary lobule, as defined by Miller, refers to the smallest unit of lung structure marginated by connective tissue septa (8,9) (Figs 1, 2). Secondary pulmonary lobules are irregularly polyhedral in shape and vary in size, measuring from 1 to 2.5 cm in diameter in most locations (8,11–14). In one study (14), the average diameter of secondary lobules measured in several adults ranged from 11 to 17 mm.

Airways, pulmonary arteries and veins, lymphatics, and the various components of the pulmonary interstitium are all represented at the level of the secondary lobule (Figs 1, 2). Each secondary lobule is supplied by a small bronchiole and pulmonary artery branch and is variably marginated in different lung regions by connective tissue, the interlobular septa, that contains pulmonary veins and lymphatics (15). Secondary lobular anatomy is easily visible on the surface of the lung because of these interlobular septa (8,11).

The pulmonary acinus is smaller than the secondary lobule. It is defined as the portion of lung distal to a terminal bronchiole (the last purely conducting airway) and is supplied by a first-order respiratory bronchiole or bronchioles (16). Since respiratory bronchioles are the largest airways that have alveoli in their walls, an acinus is the largest lung unit in which all airways participate in gas exchange. Acini are usually described as ranging from 6 to 10 mm in diameter (14,17) (Fig 1).

Secondary pulmonary lobules are usually made up of a dozen or fewer acini, although the number varies considerably in different reports (18,19). In a study by Itoh et al (10), the number of acini counted in lobules of varying sizes ranged from three to 24.

Essentials

- The secondary pulmonary lobule is a fundamental unit of lung structure, and an understanding of lobular anatomy is essential to the interpretation of thin-section CT of the lung.
- Pulmonary disease occurring predominantly in relation to interlobular septa and the periphery of lobules is termed "perilobular"; this distribution of disease may reflect abnormalities of the interlobular septa or peripheral alveoli.
- Centrilobular abnormalities visible on thin-section CT scans may consist of nodular opacities; the tree-in-bud appearance, which usually indicates the presence of a small-airways abnormality; increased visibility of centrilobular structures due to thickening or infiltration of the surrounding interstitium; or abnormal low-attenuation areas related to bronchiolar dilatation or emphysema.

Historical Considerations

Concepts regarding the importance of the secondary pulmonary lobule, acinus, and smaller lung units have evolved during the past 300 years in conjunction with continued progress in the understanding of lung anatomy, pathology, and physiology. An excellent perspective on the sequence of events and incremental discoveries made during this period has been provided by Miller (20).

The earliest detailed description (from 1676) of the secondary pulmonary lobule was provided by Thomas Willis, who studied lung structure by injecting mercury and other fluids into the bronchi and pulmonary vessels. He found that "little lobes" (ie, the lobules) arose from small branches of the trachea and were separated from each other by a "membrane" (Fig 3). Bronchioles entering the little lobes were described as dividing into a large number of fine branches, which led to minute "bladders" or "vesicles."

Georg Rindfleisch (in 1875) first used the term *acinus* to indicate a sublobular lung unit. He described the secondary lobule as supplied by a bronchiole, which divided into progressively smaller bronchiolar branches, finally giving rise to arborizing *alveolengange* (alveolar passages), which collectively formed a "lung acinus" (Fig 4). The acinus, according to Rindfleisch, was a much more consistent unit of lung structure than was the secondary lobule because of variation in the size of lobules. On the other hand, he regarded the secondary lobule to be more important than the acinus pathologically, in that disease processes tended to be limited by the connective tissue septa that marginate the lobules.

In 1881 Rudolph Kolliker, using the lung of an executed criminal, provided a more detailed analysis of the finer divisions of the bronchial tree and described respiratory bronchioles as airways that have both bronchiolar epithelium and alveoli in their walls. He distinguished respiratory bronchioles from proximal airways that do not have alveoli in their walls (ie, terminal bronchioles) and distal airways that have numerous alveoli in their walls (ie, *alveolengange,* subsequently termed alveolar ducts), thus providing the basis for defining the lung acinus relative to airway anatomy.

1947, in his book entitled *The Lung* (21), William Snow Miller reviewed lung anatomy in detail. His definitions of

Published online before print
10.1148/radiol.2392041968

Radiology 2006; 239:322–338

Originally presented at the 34th Annual Fleischner Society Conference on Chest Disease, Orlando, Fla, May 20, 2004.

the secondary pulmonary lobule and acinus are still in use today (see above). However, he also considered the primary pulmonary lobule to be a fundamental unit of lung structure. He defined the primary pulmonary lobule as all the alveolar ducts, alveolar sacs, and alveoli distal to the last respiratory bronchiole, along with their associated blood vessels, nerves, and connective tissues (Fig 5). However, since the term "primary pulmonary lobule" is not in common use today, "secondary pulmonary lobule", "secondary lobule", and "lobule" are often used interchangeably; in general, they should be considered as synonymous.

In 1958, Reid suggested an alternate definition of the secondary pulmonary lobule based on the branching pattern of peripheral bronchioles identified bronchographically rather than on the presence and location of connective tissue septa (16,19). On bronchographic images, small bronchioles can be seen to arise at intervals of 5–10 mm from larger airways; these small bronchioles show branching at approximately 2-mm intervals, the so-called millimeter pattern (16). Airways that show the millimeter pattern were considered by Reid to be intralobular, with each branch corresponding to a terminal bronchiole (19). She considered lobules to be the lung units supplied by three to five of the millimeter-pattern bronchioles. Although Reid's criteria delineate lung units of approximately equal size, about 1 cm in diameter and containing three to five acini, it should be understood that this definition does not necessarily describe lung units equivalent to the secondary lobules as defined by Miller and marginated by interlobular septa (10,19). Miller's definition is most applicable to the interpretation of thin-section CT studies and is widely accepted by both anatomists and pathologists because interlobular septa are visible on histologic sections (10).

A foundation for our current understanding of secondary lobular anatomy and its importance in radiographic interpretation was provided by Heitzman and colleagues in two articles published in 1969 (11,15) and subsequently detailed in his book entitled *The Lung: Radiologic-Pathologic Correlations* (22). Heitzman described the radiographic appearances of various lobular abnormalities, as carefully correlated with inflated and fixed lung specimens. In the initial articles (11,15), Heitzman et al described the appearance of septal thickening associated with fibrosis or lymphatic and pulmonary venous abnormalities, as well as panlobular consolidation in pulmonary infarction and bronchopneumonia. In the later and more detailed descriptions, Heitzman (22) further emphasized the radiographic appearances of the lobular "core" structures and demonstrated the radiographic and pathologic findings of peribronchiolar nodules and sublobular opacities, which are now generally referred to by using the term "centrilobular."

Thin-Section CT Appearances of the Secondary Lobule

On thin-section CT images, the secondary pulmonary lobule may be thought of as having three primary components: the interlobular septa and septal structures, the centrilobular region and centrilobular structures, and the lobular parenchyma.

Interlobular Septa and Septal Structures

Secondary lobules are marginated by the connective-tissue interlobular septa, which extend inward from the pleural surface. The interlobular septa are part of the peripheral interstitial fiber system described by Weibel (12). The peripheral interstitium extends over the surface of the lung beneath the visceral pleura and envelopes the lung in a fibrous sac from which the connective-tissue septa penetrate the lung parenchyma. Pulmonary veins and lymphatics lie within the connective-tissue interlobular septa (Figs 1, 2).

Secondary pulmonary lobules in the lung periphery are relatively large and are marginated by interlobular septa that are thicker and better defined than lobules in other parts of the lung (15,23). Peripheral lobules tend to be relatively uniform in appearance, often having a cuboidal or pyramidal shape (15). Secondary lobules in the central lung zone are smaller and more irregular in shape than those in the peripheral lung and are marginated by interlobular septa that are thinner and less well defined. When visible, lobules in the central lung zone may appear hexagonal or polygonal in shape. It should be kept in mind, however, that the size, shape, and appearance of secondary lobules as seen on thin-section CT images are markedly affected by their orientation relative to the scan plane.

Interlobular septa are thickest and most numerous in the apical, anterior, and lateral aspects of the upper lobes, the anterior and lateral aspects of the

Figure 1

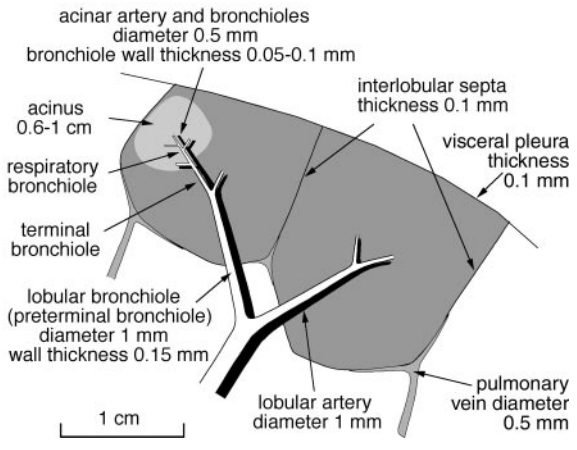

Figure 1: Diagram shows anatomy and dimensions of secondary lobule and pulmonary acinus. Two secondary pulmonary lobules in the lung periphery are illustrated, with approximate dimensions of their components indicated.

middle lobe and lingula, the anterior and diaphragmatic surfaces of the lower lobes, and along the mediastinal pleural surfaces (24); thus, secondary lobules are best defined in these regions. Septa measure about 100 μm (0.1 mm) in thickness in a subpleural location (1,4, 5,12).

Interlobular septa in the peripheral lung are at the lower limit of thin-section CT resolution (5). In healthy patients, a few septa are often visible in the lung periphery, but they tend to be inconspicuous; normal septa are most often seen in areas where they are best developed; namely, in the apices anteriorly and along the mediastinal pleural surfaces (3,25). Occasionally, when interlobular septa are not clearly visible, their locations can be inferred by identifying septal pulmonary vein branches, approximately 0.5 mm in diameter. Veins can sometimes be seen as linear, arcuate, or branching structures 1.0–1.5 cm from the pleural surface or surrounding centrilobular arteries and approximately 5–10 mm from the arteries. Pulmonary veins may also be identified by their pattern of branching; it is common for small veins to arise at nearly right angles to a much larger main branch.

Centrilobular Region and Centrilobular Structures

The bronchiole supplying a pulmonary lobule is best called the "lobular" bronchiole. It represents a preterminal bronchiole (a general term) and gives rise, in succeeding generations of branching, to smaller preterminal bronchioles, terminal bronchioles, and respiratory bronchioles. The central portion of the secondary pulmonary lobule, or the centrilobular region, contains the pulmonary artery and bronchiolar branches (ie, preterminal, terminal, and respiratory bronchioles) that supply the lobule, as well as lymphatics and supporting connective tissue (1,4,5,8,12) (Figs 1, 2). It is difficult to define lobules precisely in relation to the bronchial or arterial trees; lobules do not arise at a specific branching generation or from a specific type of bronchiole or artery (8).

Branching of the lobular bronchiole and artery is irregularly dichotomous (10). Most often, bronchioles and arteries divide into two branches of different sizes, one branch being nearly the same size as the one it arose from and the

Figure 2

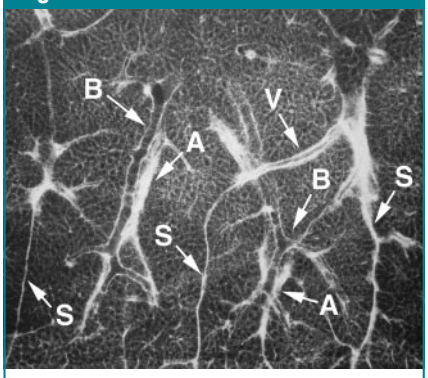

Figure 2: Radiograph of 1-mm lung slice taken from peripheral lower lobe. Two well-defined secondary pulmonary lobules are visible. Lobules are marginated by thin interlobular septa *(S)* containing pulmonary vein *(V)* branches. Bronchioles *(B)* and pulmonary arteries *(A)* are centrilobular. (Reprinted, with permission, from reference 10.)

Figure 3

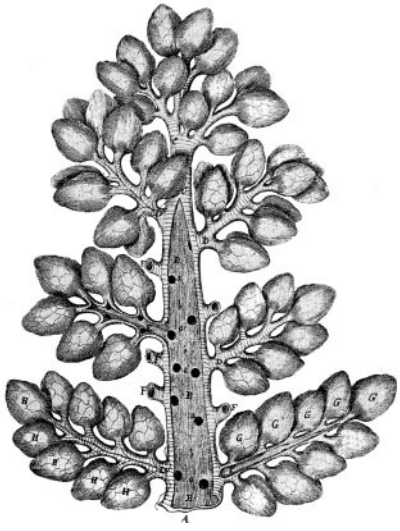

Figure 3: Secondary pulmonary lobules according to Thomas Willis (*De respirationis organis et usu.* In: *Opera omnia.* Geneva, Switzerland, 1676). Drawing shows a number of secondary lobules arising from small bronchial branches.

Figure 4

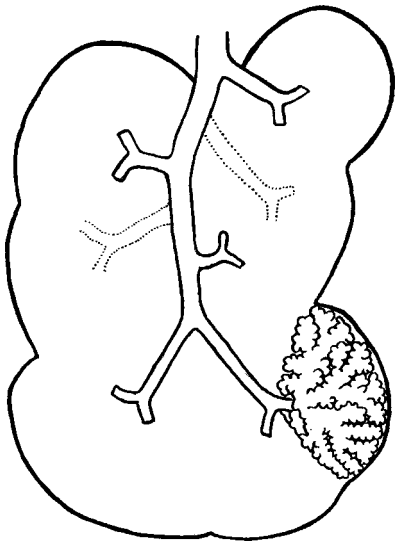

Figure 4: Secondary pulmonary lobule and acinus as shown by Georg Rindfleisch. The lobular bronchiole is shown dividing into smaller branches, which supply the acini.

Figure 5

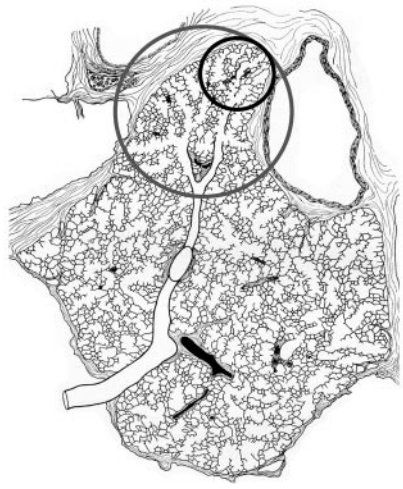

Figure 5: Secondary pulmonary lobule, as shown by Miller. Diagram shows secondary pulmonary lobule from lung periphery surrounded by connective-tissue septa and pulmonary vein branches. Also shown is airway anatomy from the level of the lobular bronchiole to lung periphery. Large circle shows approximate size of an acinus. Smaller circle shows approximate size of a primary pulmonary lobule as defined by Miller. Pulmonary artery branches are shown as thick black structures. (Reprinted, with permission, from reference 21.)

Figure 6

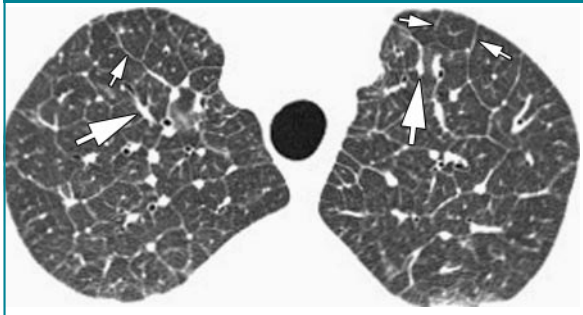

Figure 6: Interlobular septal thickening in pulmonary edema. Transverse thin-section CT scan shows thickened septa (small arrows) in upper lobes. Smooth thickening of interlobular septa outline a number of secondary pulmonary lobules. Visible lobules vary in size, at least partly because of the position of lobules relative to the scan plane. Pulmonary veins (large arrows) in septa are visible as small rounded dots or linear or branching opacities. Septa are well developed in the apices, and septal thickening is often well depicted in this region.

other being smaller. Thus, on thin-section CT scans, there often appears to be a single dominant bronchiole or artery in the center of the lobule, with smaller branches emerging at intervals along its length.

Secondary lobules are supplied by arteries and bronchioles measuring approximately 1 mm in diameter, while intralobular terminal bronchioles and arteries measure about 0.7 mm in diameter and acinar bronchioles and arteries range from 0.3 mm to 0.5 mm in diameter (Figs 1, 2). Arteries of this size can be easily resolved by using thin-section CT (4,5). On thin-section CT scans, a linear, branching, or dotlike opacity seen in the center of a lobule or within 1 cm of the pleural surface represents the intralobular artery branch or its divisions (1,4,5). The smallest arteries resolved extend to within 3–5 mm of the pleural surface or lobular margin and are as small as 0.2 mm in diameter (1,4,5).

The visibility of bronchioles in healthy subjects depends on the wall thickness of the bronchiole, rather than its diameter. For a 1-mm bronchiole supplying a secondary lobule, the wall thickness measures approximately 0.15 mm; this is at the lower limit of thin-section CT resolution. The wall of a terminal bronchiole measures only 0.1 mm in thickness, and that of an acinar bronchiole is only 0.05 mm, both of which are below the resolution of thin-section CT for a tubular structure. In one in vitro study (5), only bronchioles with a diameter of 2 mm or more or a wall thickness of more than 100 μm were visible at thin-section CT, and resolution is certainly less than this for most clinical scanners. It is important to remember that with clinical thin-section CT, intralobular bronchioles are not normally visible, and bronchi or bronchioles are rarely seen within 1 cm of the pleural surface in most locations (26,27).

The peribronchovascular interstitium is a system of fibers that invests bronchi and pulmonary arteries and forms a strong connective-tissue sheath that surrounds these structures in the perihilar lung (28). The more peripheral continuum of this interstitial fiber system surrounds small centrilobular bronchioles and arteries. Taken together, they correspond to the "axial fiber system" described by Weibel (12), which extends peripherally from the pulmonary hila to the level of the alveolar ducts and sacs.

Lobular Parenchyma and Lung Acini

The substance of the secondary lobule, which surrounds the centrilobular region and is contained within the interlobular septa, consists of functioning lung parenchyma—namely, alveoli and the associated pulmonary capillary bed supplied by small airways and branches of the pulmonary arteries, veins, and lymphatics. This parenchyma is supported by a connective-tissue stroma, a fine network of very thin fibers within the alveolar septa termed the "septal fibers" by Weibel and Taylor (8,12). On thin-section CT scans, small intralobular vascular branches are often visible within secondary lobules, but little else is visible in healthy subjects.

Lung acini are not normally visible on thin-section CT scans (10). First-order respiratory bronchioles and the acinar artery both measure about 0.5 mm in diameter; thus, intralobular acinar arteries are large enough to be seen on thin-section CT scans in some healthy subjects (8,12,14,17). Murata et al (5) showed that pulmonary artery branches as small as 0.2 mm in diameter, associated with a respiratory bronchiole and thus acinar in nature, are visible at thin-section CT and that they can extend to within 3–5 mm of the lobular margins or pleural surface.

Thin-Section CT Diagnosis of Lobular Abnormalities

Pathologic alternations in secondary lobular anatomy visible on thin-section CT scans may be described as perilobular (interlobular septal thickening and peripheral lobular diseases), centrilobular, and panlobular.

Perilobular Pattern: Interlobular Septal Thickening and Peripheral Lobular Abnormalities

Pulmonary disease occurring predominantly in relation to interlobular septa and the periphery of lobules has been called "perilobular" (29,30), although this term is not in common use. Johkoh et al (30,31) emphasized that a perilobular distribution of disease may reflect abnormalities of the interlobular septa or peripheral alveoli.

Septa easily seen on thin-section CT scans are abnormally thickened. In the peripheral lung, thickened septa 1.0–2.5 cm in length may outline part of or an entire lobule and are usually seen extending to the pleural surface (Fig 6) (1,3,5,25,32–35). Lobules delineated by thickened septa commonly contain a

Table 1

Perilobular Pattern: Differential Diagnosis

CT Finding	Differential Diagnosis
Smooth interlobular septal thickening	Pulmonary edema, hemorrhage, or veno-occlusive disease; lymphangitic spread of neoplasm; lymphangiomatosis; amyloidosis; pneumonia; alveoloar proteinosis
Nodular interlobular septal thickening	Lymphangitic spread of neoplasm, lymphoproliferative disease (eg, lymphocytic interstitial pneumonia), sarcoidosis, silicosis and coal worker's pneumoconiosis, amyloidosis
Irregular interlobular septal thickening	End-stage lung disease, sarcoidosis, usual interstitial pneumonia, asbestosis, hypersensitivity pneumonitis
Peripheral lobular abnormalities	Idiopathic pulmonary fibrosis, usual interstitial pneumonia, organizing pneumonia

Figure 7

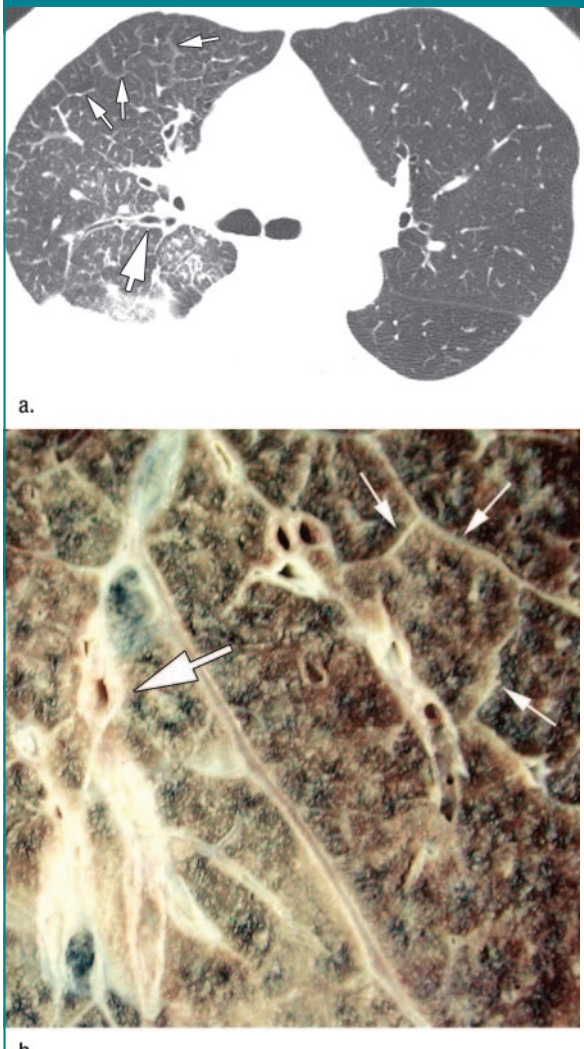

Figure 7: Interlobular septal thickening in lymphangitic spread of carcinoma. **(a)** Transverse thin-section CT scan in patient with right lung carcinoma shows smooth thickening of interlobular septa (small arrows) in the right upper lobe. Thickening of the peribronchovascular interstitium results in apparent increased thickness of right-sided bronchi (large arrow). Right pleural effusion is also present. Left lung appears normal. **(b)** Cut surface of lung in a different patient with lymphangitic spread of neoplasm. Smooth thickening of interlobular septa (small arrows) and peribronchovascular interstitium (large arrow) are seen. (Image courtesy of Martha Warnock, MD, University of California, San Francisco.)

visible dotlike or branching centrilobular pulmonary artery. The characteristic relationship of the interlobular septa and centrilobular artery or arteries is often of value for the identification of each of these structures (36).

Thickening of interlobular septa is commonly seen in patients with a variety of interstitial lung diseases, and the presence of a few thickened septa is of little diagnostic value when other CT abnormalities are also visible. When septal thickening is a predominant feature of disease, its differential diagnosis is based on its appearance. Septal thickening can be seen in the presence of interstitial fluid, cellular infiltration, or fibrosis and can have a smooth, nodular, or irregular contour in different pathologic processes (Table 1) (1,37).

smooth septal thickening

Smooth septal thickening is usually seen in association with venous, lymphatic, or infiltrative diseases. Specifically, it may reflect pulmonary edema (Fig 6) or hemorrhage (38–40); pulmonary veno-occlusive disease (38,40,41); lymphangitic spread of carcinoma (Fig 7), lymphoma, or leukemia (33,35,42); lymphoproliferative disease; lymphangiomatosis (43,44); interstitial infiltration associated with amyloidosis (45); and some pneumonias. Smooth septal thickening may also be seen in association with ground-glass opacity, a pattern termed "crazy paving"; this pattern is typical of alveolar proteinosis but has an extensive differential diagnosis (31,46–49).

nodular septal thickening

Nodular or "beaded" septal thickening (42) typically occurs in lymphatic or infiltrative diseases, including lymphangitic spread of carcinoma or lymphoma (33,35,42), lymphoproliferative disease such as lymphocytic interstitial pneumonia (50–52), sarcoidosis (53–56), silicosis or coal worker's pneumoconiosis (anthracosilicosis) (57), and amyloidosis (45,58) (Fig 8).

The presence of septal nodules is often associated with a so-called perilymphatic or lymphatic distribution of nodules, in which abnormalities occur primarily in relation to pulmonary lym-

phatics (36,44,54,59). In addition to septal nodules, a perilymphatic pattern is associated with interstitial thickening or nodules involving *(a)* the subpleural regions, *(b)* the peribronchovascular interstitium in a perihilar location, and *(c)* the centrilobular peribronchovascular interstitium. This pattern is most typical of patients with sarcoidosis, lymphangitic spread of carcinoma or other neoplasms, and lymphoproliferative disease.

irregular septal thickening

Although interlobular septal thickening can be seen on thin-section CT scans in association with fibrosis and honeycombing (60), it is not usually a predominant feature (34,61,62). Generally speaking, in the presence of substantial fibrosis and honeycombing, distortion of lung architecture makes the recognition of lobules and thickened septa difficult. Among patients with pulmonary fibrosis and end-stage lung disease, the presence of interlobular septal thickening on thin-section CT scans is most frequent in patients with sarcoidosis and is less common in those with usual interstitial pneumonia of various causes, asbestosis, or hypersensitivity pneumonitis (62). The frequency of septal thickening and fibrosis in patients with sarcoidosis reflects the tendency of active sarcoid granulomas to involve the interlobular septa. In patients who have interstitial fibrosis, septal thickening visible on thin-section CT scans is often irregular in appearance or associated with marked distortion of lung structures (4).

peripheral lobular abnormalities

In patients with idiopathic pulmonary fibrosis or usual interstitial pneumonia of other cause, irregular reticular opacities are often visible on thin-section CT scans; these opacities appear to represent thickened interlobular septa (Fig 9). This finding usually correlates with the presence of fibrosis that predominantly affects the periphery of acini and the secondary lobule rather than the septa themselves (Fig 9) (44,61). Nonetheless, the CT appearance is similar to that of irregular septal thickening. This has been termed a peripheral lobular, or perilobular, distribution.

A similar peripheral lobular (perilobular) distribution of abnormalities has been reported in as many as half of patients with organizing pneumonia (63). These abnormalities result in a thin-section CT appearance of arcuate or polygonal opacities, which are less well defined than thickened septa. Although the histologic correlates of this pattern are unclear, it is likely related to organizing pneumonia involving the distal airspaces.

Centrilobular Abnormalities

Centrilobular abnormalities generally may be classified as bronchiolocentric, angiocentric, perilymphatic, or interstitial. Centrilobular abnormalities visible at thin-section CT may consist of *(a)* nodular opacities, *(b)* an appearance termed "tree-in-bud" that usually indicates the presence of a small-airways abnormality, *(c)* increased visibility of centrilobular structures due to thickening or infiltration of the interstitium surrounding them, or *(d)* abnormal areas of low attenuation related to bronchiolar dilatation or emphysema.

centrilobular nodules

Centrilobular nodules can reflect the presence of either interstitial or airspace abnormalities. The histologic correlates reported to occur in association with centrilobular nodules vary with the disease entity (64).

On thin-section CT scans, centrilobular nodules usually appear to be separated from the pleural surfaces, fissures, and interlobular septa by a distance of at least several millimeters (Fig 10). In the lung periphery, the nodules are usually centered 5–10 mm from the pleural surface, a fact that reflects their centrilobular origin. Although centrilobular nodules, when large, may touch the pleural surface, they do not appear to arise at the pleural surface.

Centrilobular nodules may be dense and of homogeneous attenuation or of ground-glass opacity. They may range from a few millimeters to a centimeter in size. Either a single centrilobular nodule or a centrilobular rosette of nodules

Figure 8

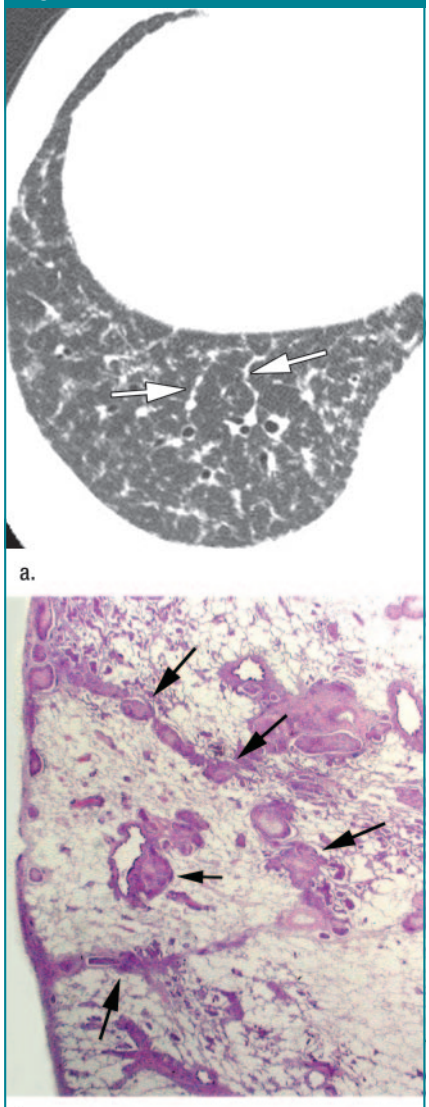

Figure 8: Nodular thickening of interlobular septa. **(a)** Transverse thin-section CT scan at level of right lung base in a patient with sarcoidosis shows interlobular septal thickening associated with several septal nodules (arrows). **(b)** Histologic specimen in patient with lymphangitic spread of tumor shows secondary pulmonary lobule with nodules of tumor (large arrows) in the interlobular septa. Tumor (small arrow) is also visible in centrilobular peribronchovascular region. (Hematoxylin-eosin stain; original magnification, ×10.) (Image courtesy of Kirk Jones, MD, University of California, San Francisco.)

Table 2

Centrilobular Nodules: Differential Diagnosis

Cause	Differential Diagnosis
Bronchiolar infection	Endobronchial spread of tuberculosis, nontuberculous mycobacteria or other granulomatous infection, bronchopneumonia, infectious bronchiolitis, cystic fibrosis
Bronchioloar inflammation	Hypersensitivity pneumonitis, diffuse panbronchiolitis, asthma, allergic bronchopulmonary aspergillosis, Langerhans cell histiocytosis, organizing pneumonia, bronchiolitis obliterans, respiratory bronchiolitis in smokers, asbestosis, follicular bronchiolitis
Endobronchial spread of tumor	For example, bronchioloalveoloar carcinoma
Angiocentric disease	Pulmonary edema, pulmonary vasculitis, talcosis, pulmonary hemorrhage or hemosiderosis, metastatic calcification, pulmonary hypertension
Perilymphatic disease	Sarcoidosis, silicosis and coal worker's pneumoconiosis, lymphangitic spread of neoplasm, lymphocytic interstitial pneumonia

Figure 9

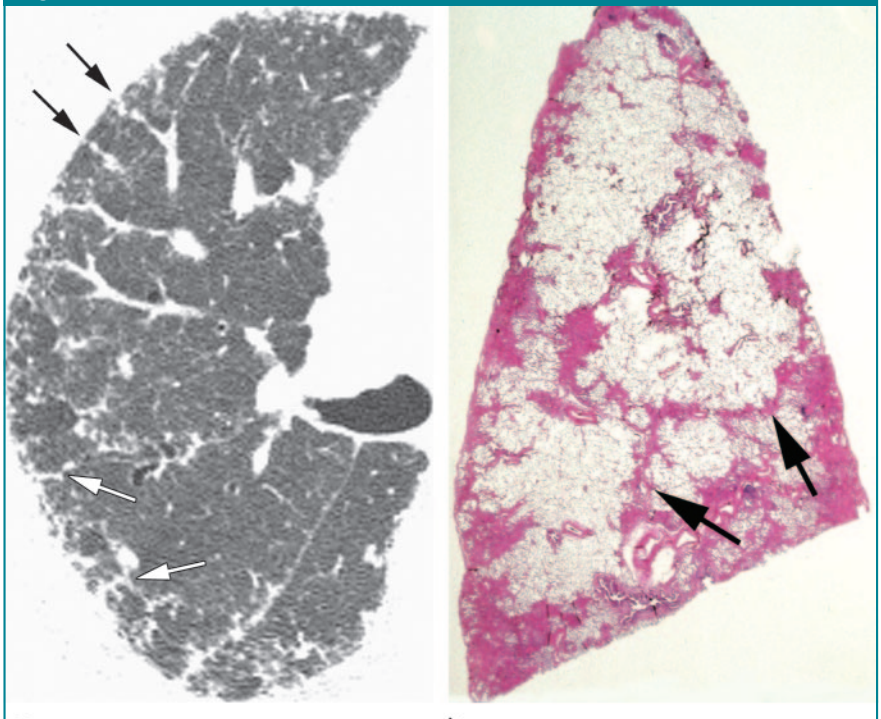

a. b.

Figure 9: Peripheral lobular fibrosis in idiopathic pulmonary fibrosis. **(a)** Transverse thin-section CT scan through right upper lobe in a patient with idiopathic pulmonary fibrosis shows irregular reticular opacities (arrows). **(b)** Histologic specimen from open lung biopsy in a different patient with idiopathic pulmonary fibrosis shows irregular fibrosis (arrows) in periphery of secondary pulmonary lobules. (Hematoxylin-eosin stain; original magnification, ×4.)

may be visible (5,65,66). Although centrilobular nodules are often ill defined, this is not always the case. Because of the similar size of secondary lobules, centrilobular nodules often appear to be evenly spaced. They may appear patchy or diffuse in different diseases.

The term *centrilobular nodules* is best thought of as indicating that the nodules are seen to be related to centrilobular structures, even if they cannot be precisely localized to the centers of secondary lobules. Indeed, in many cases, centrilobular nodules can be identified by noting their association with small pulmonary artery branches. In occasional cases, an air-filled centrilobular bronchiole can be recognized as a rounded area of low attenuation within a centrilobular nodule (Fig 11).

Centrilobular nodules are most commonly seen in patients with disease that primarily affects centrilobular bronchioles and results in inflammation, infiltration, or fibrosis of the surrounding interstitium and alveoli (Table 2) (44,64). The differential diagnosis of this appearance is long, but most diseases resulting in centrilobular nodules are associated with so-called cellular bronchiolitis, defined histologically by the presence of inflammatory cell infiltrates involving the bronchiolar wall and lumen. Infectious diseases associated with cellular bronchiolitis and centrilobular nodules include endobronchial spread of tuberculosis, nontuberculous mycobacteria, or other granulomatous infections (5,29,66–69); bronchopneumonia; infectious bronchiolitis (70); and cystic fibrosis. Noninfectious inflammatory diseases of bronchioles associated with cellular bronchiolitis and centrilobular nodules include hypersensitivity pneumonitis (Fig 10) (71–74), diffuse panbronchiolitis (Fig 11) (75–77), asthma and allergic bronchopulmonary aspergillosis (78), Langerhans cell histiocytosis (79), organizing pneumonia (80,81), bronchiolitis obliterans (64,82), respiratory bronchiolitis in smokers (83–86), asbestosis (87), and follicular bronchiolitis (88–91). Endobronchial spread of neoplasm, usually bronchioloalveolar carcinoma may also result in this appearance in some patients (92,93).

Angiocentric diseases are less common than bronchiolitis as a cause of centrilobular nodules. Causes include pulmonary edema (39,66,94); pulmonary vasculitis, including that related to injected substances such as talc (64,95, 96); pulmonary hemorrhage or hemosiderosis (97,98); metastatic calcification (99,100); and vascular lesions associated with pulmonary hypertension (41,101).

Centrilobular nodules also can be seen in diseases associated with a perilymphatic distribution of abnormalities; these diseases include sarcoidosis, silicosis, and lymphangitic spread of tumor (Fig 8) (29,53,54). In some cases, centrilobular clusters of granulomas are a predominant feature of sarcoidosis. Small centrilobular nodules are also characteristic of both silicosis and coal worker's pneumoconiosis (57,96); this abnormality may be considered peribronchiolar as well as perilymphatic. In patients with lymphangitic spread of carcinoma (although interlobular septal thickening is usually a predominant feature of the disease), centrilobular peribronchovascular interstitial thickening or nodules is commonly seen (64). Lymphocytic interstitial pneumonia can result in the presence of ill-defined centrilobular opacities (50,52).

Figure 10

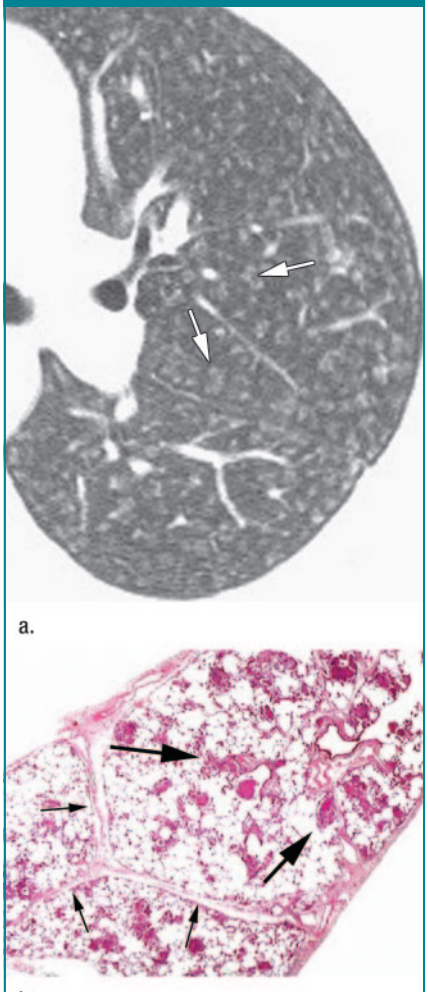

Figure 10: Centrilobular nodules in hypersensitivity pneumonitis. **(a)** Transverse thin-section CT scan shows small ill-defined centrilobular nodules separated from pleural surface and fissure by several millimeters. The nodules arise in relation to centrilobular bronchioles and appear as lobular rosettes (arrows). **(b)** Histologic specimen shows ill-defined peribronchiolar and alveolar infiltrates (large arrows) that predominate in center of a secondary lobule. Interlobular septa (small arrows) outline parts of three lobules. (Hematoxylin-eosin stain; original magnification, ×15.) (Image courtesy of Martha Warnock, MD, University of California, San Francisco.)

Figure 11

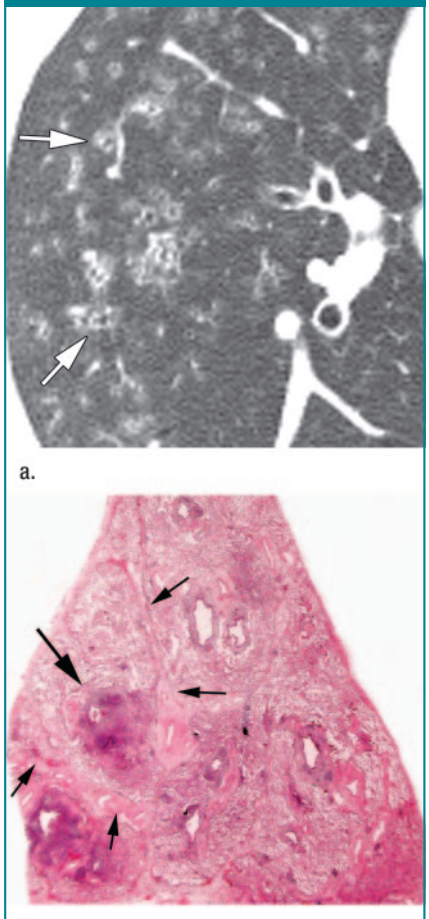

Figure 11: Centrilobular nodules and abnormal airways in cellular bronchiolitis. **(a)** Transverse thin-section CT scan in a patient with follicular bronchiolitis shows small ill-defined centrilobular nodules. In some locations (arrows), these are seen to surround dilated centrilobular bronchioles. The cause of bronchiolitis in this patient was not determined. **(b)** Histologic specimen from open lung biopsy in a patient with diffuse panbronchiolitis. Small arrows outline a secondary lobule. Peribronchiolar infiltrates (large arrow) predominate in centers of several secondary lobules. Centrilobular bronchioles are dilated. (Hematoxylin-eosin stain; original magnification, ×10.)

tree-in-bud sign

The tree-in-bud sign usually reflects the presence of dilated centrilobular bronchioles with lumina that are impacted with mucus, fluid, or pus; it is often associated with peribronchiolar inflammation (Fig 12) (64,67,82,102,103). Because of the branching pattern of the dilated bronchiole and the presence of ill-defined nodules of peribronchiolar inflammation, its appearance has been likened to a budding or fruiting tree (67,75) or to the child's toy jacks (103). The term "budding tree" has also been used to describe the appearance of small-airways filling at bronchography (16).

On thin-section CT scans, the tree-in-bud finding is usually easy to recognize, but several different appearances may be seen alone or in combination. In the lung periphery, the tree-in-bud sign may be associated with a typical branching appearance, with the most peripheral branches or nodular opacities being several millimeters from the pleural surface (Fig 12). The tree-in-bud sign may also appear as a centrilobular cluster of nodules, depending on the relationship of the bronchiole to the plane of the scan. If the centrilobular bronchiole is sectioned across its axis, as is typical in the costophrenic angles, the impacted bronchiole may appear to be a single

Figure 12

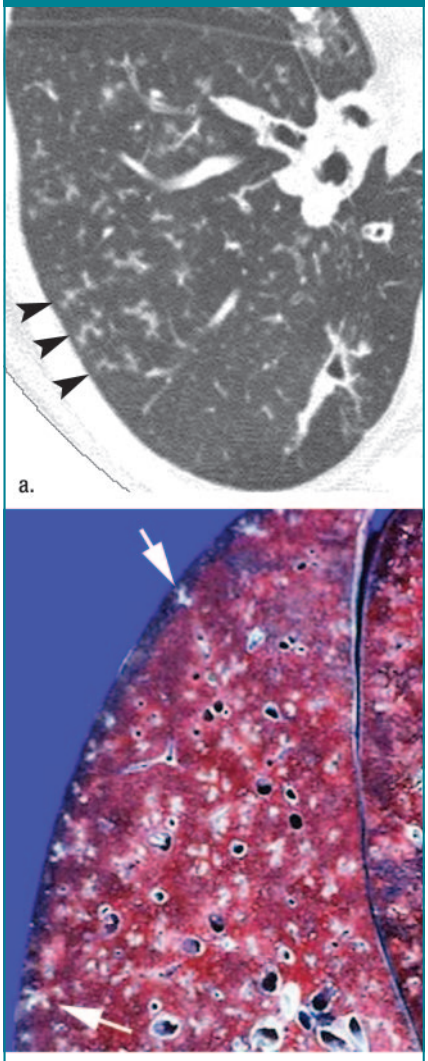

Figure 12: Tree-in-bud sign associated with bronchiolar infection. **(a)** Transverse thin-section CT scan through right lower lobe in a patient with airways disease and bacterial infection related to acquired immunodeficiency syndrome. Multiple impacted centrilobular bronchioles result in tree-in-bud appearance (arrowheads). Bronchiectasis is also present. **(b)** Lung slice from patient with bronchopneumonia. Impacted mucus- and pus-filled bronchioles (arrows) are visible throughout the lung; this is the pathologic examination equivalent of the tree-in-bud sign. (Image courtesy of Martha Warnock, MD, University of California, San Francisco.)

well-defined centrilobular nodule a few millimeters in diameter.

Abnormal bronchioles producing a tree-in-bud pattern can usually be distinguished from normal centrilobular vessels by their more irregular appearance, lack of tapering, and knobby or bulbous appearance at the tips of small branches. Normal centrilobular arteries are considerably thinner than the branching bronchioles seen in patients with the tree-in-bud sign and are much less conspicuous.

The tree-in-bud sign is usually associated with other abnormal findings visible on thin-section CT scans. Bronchiolar dilatation and wall thickening can sometimes be seen in association with the tree-in-bud pattern if the dilated bronchioles are air filled; normal bronchioles should not be visible in the peripheral 1 cm of lung. The tree-in-bud sign may also be associated with ill-defined centrilobular nodules representing areas of inflammation. Large-airways abnormalities with bronchial wall thickening or bronchiectasis are also often present (64). In a study by Aquino et al (102), 26 (96%) of 27 patients with thin-section CT findings of the tree-in-bud pattern also showed bronchiectasis or bronchial wall thickening.

The tree-in-bud finding is usually indicative of small-airways disease. Furthermore, a tree-in-bud appearance is associated with airways infection in the majority of cases, although it may also be seen in patients with mucoid impaction or bronchiolar wall infiltration (88). In one study (102), 19 (25.6%) of 74 patients with bronchiectasis and six (17.6%) of 34 patients with infectious bronchitis showed the tree-in-bud sign, but this finding was not visible in patients with other diseases that involve the small airways, such as emphysema, respiratory bronchiolitis, bronchiolitis obliterans, or hypersensitivity pneumonitis. Similarly, in 21 (72%) of 29 patients with active tuberculosis, a tree-in-bud appearance was visible (67), and it correlated with the presence of caseous material in terminal and respiratory bronchioles. In patients with diffuse panbronchiolitis, prominent branching centrilobular opacities represent dilated bronchioles with inflammatory bronchiolar wall thickening and abundant intraluminal secretions (75,76).

Thus, in patients with a centrilobular distribution of nodules, if the tree-in-bud sign can be recognized the differential diagnosis is limited: endobronchial spread of tuberculosis (67) or nontuberculous mycobacteria (64), bronchopneumonia, infectious bronchiolitis (70), cystic fibrosis (104), bronchiectasis of any cause (64,82,102), diffuse panbronchiolitis (75,76), asthma or allergic bronchopulmonary aspergillosis (82), constrictive bronchiolitis (82), follicular bronchiolitis, bronchioloalveolar carcinoma, and intravascular metastases.

The tree-in-bud sign is less frequent in airways diseases that result in the accumulation of mucus within small bronchi, such as asthma or allergic bronchopulmonary aspergillosis, and it is rarely seen in patients with constrictive bronchiolitis, which is presumably related to impaction of bronchioles (82). Constrictive bronchiolitis is characterized histologically by the presence of concentric bronchiolar fibrosis with narrowing or obliteration of the bronchiolar lumen; it is associated with the clinical syndrome referred to as bronchiolitis obliterans.

An appearance resembling the tree-in-bud sign has also been reported in patients with follicular bronchiolitis, an entity in which hyperplasia of lymphoid follicles occurs in relation to centrilobular airways; it is seen in association with collagen-vascular disease or acquired immunodeficiency syndrome (88). Bronchioloalveolar carcinoma may occasionally show the tree-in-bud pattern, although nodules are more typical (93). In some patients with sarcoidosis, nodules that occur in relation to centrilobular arteries may mimic the tree-in-bud appearance, although other typical features of sarcoidosis are usually present (64,82). Recently, this appearance has also been reported in patients with intravascular metastases involving centrilobular arteries (105,106).

prominent (increased thickness of) centrilobular structures

Increased visibility or increased thickness of otherwise normal-appearing centrilobular structures, usually the centrilobular artery, may be seen in conditions that

result in centrilobular interstitial infiltration or thickening, such as occurs in pulmonary edema, lymphangitic spread of carcinoma, amyloidosis, or diseases associated with interstitial fibrosis. This appearance is nonspecific and is usually associated with other findings of interstitial infiltration, such as interlobular septal thickening, peribronchovascular interstitial thickening, or findings of lung fibrosis.

centrilobular low attenuation

Abnormal areas of low attenuation usually reflect bronchiolectasis or centrilobular emphysema. Cavitary centrilobular nodules may also be seen.

Bronchiolectasis may be seen in patients with airways disease or lung fibrosis. Since normal centrilobular bronchioles are not visible at thin-section CT, the recognition of air-filled airways in the lung periphery usually means that that the airways are both dilated and thick walled (Fig 11). This may be seen in airways diseases such as those that cause the tree-in-bud pattern, or it may represent traction bronchiolectasis in patients with lung fibrosis. In the latter case, an abnormal reticular pattern or other findings of fibrosis will also be visible.

Centrilobular (centriacinar) emphysema is characterized histologically by areas of lung destruction occurring in relation to centriacinar bronchioles and, therefore, is located in the center of the secondary lobule or surrounding the centrilobular region. On thin-section CT scans, low-attenuation areas of emphysema are often visible in the centers of lobules and may be seen surrounding the centrilobular artery on good-quality scans (Fig 13). Multiple small areas of low attenuation predominate in the upper lobes. In most cases, the areas of low attenuation seen on CT scans in patients with centrilobular emphysema lack a visible wall, although very thin walls are occasionally visible, and are related to areas of fibrosis.

Panlobular Abnormalities

Some lung diseases result in abnormalities that involve individual lobules or groups of lobules in their entirety while adjacent lobules appear normal, giving the lung a mosaic appearance. This may result from *(a)* lobular consolidation or infiltration with increased attenuation of lobules on thin-section CT scans or *(b)* lobular low attenuation due to decreased perfusion, air trapping, or lobular destruction (Table 3).

Figure 13

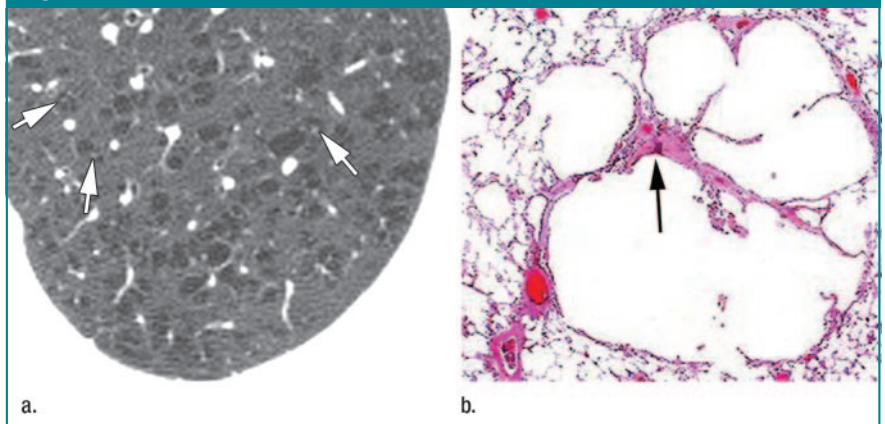

Figure 13: Centrilobular emphysema. **(a)** Transverse thin-section CT scan through left upper lobe shows a centrilobular artery (arrows) in many of the low-attenuating areas. **(b)** Histologic specimen shows areas of lung destruction surrounding a small centrilobular artery (arrow). (Hematoxylin-eosin stain; original magnification, ×10.) (Image courtesy of Martha Warnock, MD, University of California, San Francisco.)

Table 3

Panlobular Nodules: Differential Diagnosis

CT Finding	Differential Diagnosis
Lobular consolidation	Bronchopneumonia, organizing pneumonia, eosinophilic pneumonia, bronchioloalveolar carcinoma
Lobular ground-glass opacity	Bronchopneumonia, viral infection, *Pneumocystis carinii* pneumonia, *Mycoplasma pneumoniae,* pulmonary edema, hypersensitivity pneumonitis, alveolar proteinosis, lipoid pneumonia
Lobular low attenuation	Mosaic perfusion due to airways or vascular disease, emphysema (panlobular or paraseptal)
Headcheese sign	Hypersensitivity pneumonitis, desquamative interstitial pneumonia, respiratory bronchiolitis–interstitial lung disease, sarcoidosis, atypical infections with bronchiolitis (eg, *M pneumoniae*)

lobular consolidation

Lobular consolidation with a patchy distribution is typical of lobular pneumonia, also known as bronchopneumonia. Pneumonias associated with this pattern (eg, due to infection from staphylococci, *Haemophilus* species, pseudomonads, *M pneumoniae*) are characterized by thick and tenacious secretions and are spread through the airways rather than through the pores of Kohn. Infected secretions are typically present in bronchi and bronchioles. Consolidation of scattered lobules also may be seen with pulmonary embolism, which results in hemorrhage or infarction.

Chronic lung diseases that result in consolidation often involve the lung in a patchy fashion. Patchy consolidation can show a nonanatomic and nonsegmental distribution but can also be panlobular on thin-section CT scans (1,29,65,67). Eosinophilic pneumonia, organizing pneumonia, and bronchioloalveolar carcinoma may show this appearance.

lobular ground-glass opacity

As with consolidation, a variety of acute and chronic lung diseases may result in lobular areas of ground-glass opacity, which give the lung a mosaic appearance. Lobular ground-glass opacity (Fig 14) may be seen in patients with infection (eg, bronchopneumonia, viral infections, *P carinii* pneumonia, or *M pneumoniae*) (107,108), pulmonary edema (39), and chronic infiltrative diseases such hypersensitivity pneumonitis, alveolar proteinosis (31,48,109, 110), and lipoid pneumonia (111–114).

In some patients with lobular ground-glass opacity visible on thin-section CT scans, superimposition of a reticular pattern results in the crazy-paving appearance (46). This pattern was first recognized in patients with pulmonary alveolar proteinosis (46) and is quite typical of this disease; however, the crazy-paving pattern may also be seen in patients with a variety of other diseases (31,49). In patients with the crazy-paving pattern, ground-glass opacity may reflect the presence of airspace or interstitial abnormalities; the reticular opacities may represent thickening of interlobular septa, thickening of the intralobular interstitium, irregular areas of fibrosis, or a preponderance of an airspace filling process at the periphery of lobules or acini (31).

The differential diagnosis of the crazy-paving pattern includes diseases considered to be primarily airspace or interstitial and mixed conditions (31,49). These include pulmonary alveolar proteinosis (46,48); pulmonary edema (39); pulmonary hemorrhage (97); adult respiratory distress syndrome (49); acute interstitial pneumonia; diffuse alveolar damage; pneumonias due to infection by *P carinii,* virus (eg, cytomegalovirus), *Mycoplasma* species, bacteria, and tuberculosis; organizing pneumonia; chronic eosinophilic pneumonia; acute eosinophilic pneumonia (115); Churg-Strauss syndrome (116); radiation pneumonitis (117); drug-related pneumonitis; bronchioloalveolar carcinoma (118); and lipoid pneumonia (114). Clearly, the differential diagnosis of a crazy-paving pattern must be based on a consideration of clinical as well as thin-section CT findings.

lobular low attenuation due to mosaic perfusion

Lung attenuation is partially determined by the amount of blood present in lung tissue. On thin-section CT scans, inhomogeneous lung opacity can result from regional differences in lung perfusion in patients with airways obstruction or pulmonary vascular obstruction (104, 119,120). Because this phenomenon is often patchy or mosaic in distribution, with adjacent areas of lung being of differing attenuation, it has been termed "mosaic perfusion" (36,59). Areas of relatively decreased lung opacity seen at thin-section CT can be of varying sizes but commonly appear to correspond to lobules.

Mosaic perfusion is most frequent in patients with airways diseases that result in focal air-trapping or poor ventilation of lung parenchyma (104,119,120); in these patients, areas of poorly ventilated lung are poorly perfused because of reflex vasoconstriction or a permanent reduction in the pulmonary capillary bed. This finding is most common in patients with bronchiolitis obliterans, cystic fibrosis, and hypersensitivity pneumonitis (Fig 15) (121–123). Mosaic perfusion has also been reported in association with pulmonary vascular obstruction such as that caused by chronic pulmonary embolism (124–126). However, areas of low attenuation are often larger than lobules in patients with vascular abnormalities. In a study of 48 consecutive patients with lobular areas of low attenuation visible on thin-section CT scans (127), only one had isolated vascular disease; in the remainder, airways disease was the likely cause.

When mosaic perfusion is present, pulmonary vessels in the areas of decreased opacity often appear smaller than vessels in areas of relatively high attenuation in the lung (120,126). This difference reflects disparities in regional blood flow and can be quite helpful in distinguishing mosaic perfusion from lobular ground-glass opacity, which can otherwise have a similar mosaic appearance. In patients with ground-glass opacity, vessels usually appear equal in size throughout the lung. For example, in a series of 48 patients with mosaic perfusion primarily due to airway disease, Im et al (127) observed smaller vessels in areas of low attenuation in 45 (93.8%) patients. It must be pointed out, however, that decreased vessel size

Figure 14

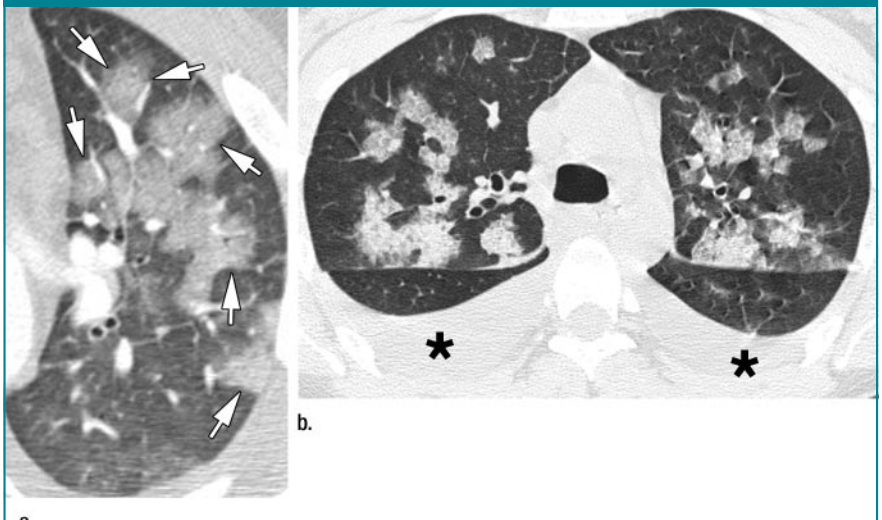

Figure 14: Transverse thin-section CT of lobular ground-glass opacity. **(a)** Contrast material–enhanced scan shows lobular pneumonia (bronchopneumonia), with lobular areas of ground-glass opacity (arrows) in left upper lobe. Centrilobular bronchioles and arteries are visible within some lobular opacities. **(b)** Lobular ground-glass opacity in a patient with pulmonary edema. Pleural effusions (*) are also present.

may be subtle and difficult to observe in some patients with mosaic perfusion. In a study by Arakawa et al (128) of patients with inhomogeneous lung opacity of various causes, only 68% of patients with airways or vascular disease were thought to show small vessels in areas of low attenuation.

Expiratory thin-section CT scans may be useful in the differentiation of lobular mosaic perfusion from lobular ground-glass opacity (128). In patients with ground-glass opacity, expiratory thin-section CT typically demonstrates a proportional increase in attenuation both in areas of increased opacity and in areas of decreased opacity. In patients with mosaic perfusion resulting from airways disease or pulmonary embolism, attenuation differences are often accentuated at expiration. Relatively high-attenuation areas increase in attenuation, while regions of lower attenuation remain low attenuating (ie, air trapping is present) (120,129–132).

mixed disease and the headcheese sign

In some patients, thin-section CT shows a patchy pattern of variable lung attenuation. This pattern represents the combination of lobular areas of ground-glass opacity (or consolidation), normal lung, and lobular areas of reduced lung attenuation indicating mosaic perfusion. This combination of mixed abnormalities, including the presence of both ground-glass opacity and mosaic perfusion, often gives the lung a geographic appearance and has been termed the "headcheese sign" (Fig 16) because of its resemblance to the variegated appearance of a sausage made from parts of the head of a hog (133). The headcheese sign is distinguished from mosaic perfusion alone by the presence of areas of increased attenuation. It can be distinguished from patchy ground-glass opacity or consolidation by the presence of air trapping. Air trapping is commonly visible on expiratory scans in patients with the headcheese sign.

The headcheese sign is indicative of mixed infiltrative and obstructive disease, usually associated with bronchiolitis. In patients with this appearance, the presence of ground-glass opacity or consolidation is due to lung infiltration, while the presence of mosaic perfusion with decreased vessel size is usually due to small-airways obstruction.

Figure 15

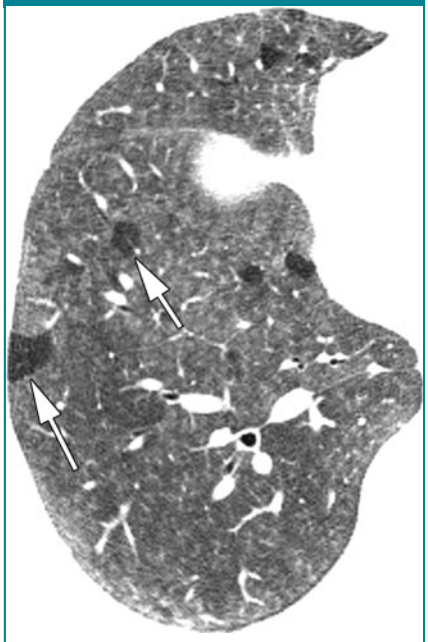

Figure 15: Lobular low attenuation in hypersensitivity pneumonitis. Transverse thin-section CT scan shows low-attenuating regions (arrows), which reflect mosaic perfusion due to air trapping. Ground-glass opacity is also present.

The most common causes of this pattern are hypersensitivity pneumonitis, desquamative interstitial pneumonia or respiratory bronchiolitis–interstitial lung disease, sarcoidosis, and atypical infections with associated bronchiolitis, such as occurs with *M pneumoniae* (107,108,133). Each of these diseases results in infiltrative abnormalities and may be associated with airways abnormalities.

lobular low attenuation due to emphysema

Panlobular emphysema results in uniform destruction of the secondary lobule, but lung involvement is usually diffuse and thin-section CT shows an overall decrease in lung attenuation and a reduction in size of pulmonary vessels, without focal areas of lobular low attenuation being seen. Paraseptal (distal acinar) emphysema results in the presence of subpleural low-attenuation areas, which often share very thin walls that are visible on thin-section CT scans. Paraseptal emphysema reflects the presence of destruction of subpleural secondary lobules marginated by interlobular septa.

Figure 16

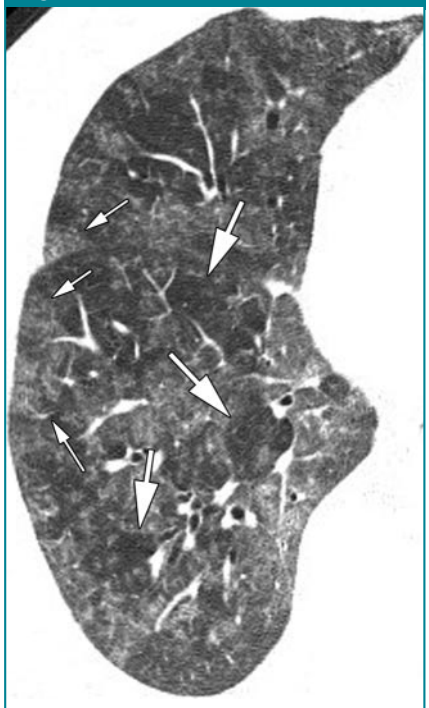

Figure 16: Headcheese sign in hypersensitivity pneumonitis. Transverse thin section CT scan shows lung with a geographic appearance, which represents a combination of patchy or lobular ground-glass opacity (small arrows) and mosaic perfusion (large arrows).

Summary

The secondary pulmonary lobule is a fundamental unit of lung structure, and the recognition of abnormalities relative to lobular anatomy is important in the diagnosis and differential diagnosis of lung abnormalities by using thin-section CT scans.

References

1. Webb WR. High-resolution CT of the lung parenchyma. Radiol Clin North Am 1989; 27:1085–1097.

2. Zerhouni EA, Naidich DP, Stitik FP, Khouri

NF, Siegelman SS. Computed tomography of the pulmonary parenchyma. II. Interstitial disease. J Thorac Imaging 1985;1:54–64.

3. Zerhouni E. Computed tomography of the pulmonary parenchyma: an overview. Chest 1989;95:901–907.

4. Webb WR, Stein MG, Finkbeiner WE, Im JG, Lynch D, Gamsu G. Normal and diseased isolated lungs: high-resolution CT. Radiology 1988;166:81–87.

5. Murata K, Itoh H, Todo G, et al. Centrilobular lesions of the lung: demonstration by high-resolution CT and pathologic correlation. Radiology 1986;161:641–645.

6. Bergin C, Roggli V, Coblentz C, Chiles C. The secondary pulmonary lobule: normal and abnormal CT appearances. AJR Am J Roentgenol 1988;151:21–25.

7. Hruban RH, Meziane MA, Zerhouni EA, et al. High resolution computed tomography of inflation fixed lungs: pathologic-radiologic correlation of centrilobular emphysema. Am Rev Respir Dis 1987;136:935–940.

8. Weibel ER, Taylor CR. Design and structure of the human lung. In: Fishman AP, ed. Pulmonary diseases and disorders. 2nd ed. New York, NY: McGraw-Hill, 1988; 11–60.

9. Miller WS. The lung. Springfield, Ill: Thomas, 1947; 39–42.

10. Itoh H, Murata K, Konishi J, Nishimura K, Kitaichi M, Izumi T. Diffuse lung disease: pathologic basis for the high-resolution computed tomography findings. J Thorac Imaging 1993;8:176–188.

11. Heitzman ER, Markarian B, Berger I, Dailey E. The secondary pulmonary lobule: a practical concept for interpretation of chest radiographs. II. Application of the anatomic concept to an understanding of roentgen pattern in disease states. Radiology 1969; 93:513–519.

12. Weibel ER. Looking into the lung: what can it tell us? AJR Am J Roentgenol 1979;133: 1021–1031.

13. Raskin SP. The pulmonary acinus: historical notes. Radiology 1982;144:31–34.

14. Osborne DR, Effmann EL, Hedlund LW. Postnatal growth and size of the pulmonary acinus and secondary lobule in man. AJR Am J Roentgenol 1983;140:449–454.

15. Heitzman ER, Markarian B, Berger I, Dailey E. The secondary pulmonary lobule: a practical concept for interpretation of chest radiographs. I. Roentgen anatomy of the normal secondary pulmonary lobule. Radiology 1969;93:507–512.

16. Reid L, Simon G. The peripheral pattern in the normal bronchogram and its relation to peripheral pulmonary anatomy. Thorax 1958;13:103–109.

17. Gamsu G, Thurlbeck WM, Macklem PT, Fraser RG. Peripheral bronchographic morphology in the normal human lung. Invest Radiol 1971;6(3):161–170.

18. Weibel ER. High resolution computed tomography of the pulmonary parenchyma: anatomical background. Presented at the Fleischner Society Symposium on Chest Disease, Scottsdale, Ariz, April 21, 1990.

19. Reid L. The secondary pulmonary lobule in the adult human lung, with special reference to its appearance in bronchograms. Thorax 1958;13:110–115.

20. Miller WS. The lung. Springfield, Ill: Thomas, 1947; 162–202.

21. Miller WS. The lung. Springfield, Ill: Thomas, 1947; 204.

22. Heitzman ER. The lung: radiologic-pathologic correlations. St Louis, Mo: Mosby, 1984.

23. Fleischner FG. The butterfly pattern of pulmonary edema. In: Simon M, Potchen EJ, LeMay M, eds. Frontiers of pulmonary radiology. New York, NY: Grune & Stratton, 1969; 360–379.

24. Reid L, Rubino M. The connective tissue septa in the foetal human lung. Thorax 1959;14:3–13.

25. Aberle DR, Gamsu G, Ray CS, Feuerstein IM. Asbestos-related pleural and parenchymal fibrosis: detection with high-resolution CT. Radiology 1988;166:729–734.

26. Kim JS, Müller NL, Park CS, Grenier P, Herold CJ. Cylindrical bronchiectasis: diagnostic findings on thin-section CT. AJR Am J Roentgenol 1997;168:751–754.

27. Kang EY, Miller RR, Müller NL. Bronchiectasis: comparison of preoperative thin-section CT and pathologic findings in resected specimens. Radiology 1995; 195:649–654.

28. Murata K, Takahashi M, Mori M, et al. Peribronchovascular interstitium of the pulmonary hilum: normal and abnormal findings on thin-section electron-beam CT. AJR Am J Roentgenol 1996;166:309–312.

29. Murata K, Khan A, Herman PG. Pulmonary parenchymal disease: evaluation with high-resolution CT. Radiology 1989;170:629–635.

30. Johkoh T, Müller NL, Ichikado K, Nakamura H, Itoh H, Nagareda T. Perilobular pulmonary opacities: high-resolution CT findings and pathologic correlation. J Thorac Imaging 1999;14:172–177.

31. Johkoh T, Itoh H, Müller NL, et al. Crazy-paving appearance at thin-section CT: spectrum of disease and pathologic findings. Radiology 1999;211:155–160.

32. Swensen SJ, Aughenbaugh GL, Brown LR. High-resolution computed tomography of the lung. Mayo Clin Proc 1989;64:1284–1294.

33. Stein MG, Mayo J, Müller N, Aberle DR, Webb WR, Gamsu G. Pulmonary lymphangitic spread of carcinoma: appearance on CT scans. Radiology 1987;162:371–375.

34. Müller NL, Miller RR, Webb WR, Evans KG, Ostrow DN. Fibrosing alveolitis: CT-pathologic correlation. Radiology 1986; 160:585–588.

35. Munk PL, Müller NL, Miller RR, Ostrow DN. Pulmonary lymphangitic carcinomatosis: CT and pathologic findings. Radiology 1988;166: 705–709.

36. Austin JH, Müller NL, Friedman PJ, et al. Glossary of terms for CT of the lungs: recommendations of the Nomenclature Committee of the Fleischner Society. Radiology 1996;200:327–331.

37. Kang EY, Grenier P, Laurent F, Müller NL. Interlobular septal thickening: patterns at high-resolution computed tomography. J Thorac Imaging 1996;11:260–264.

38. Cassart M, Genevois PA, Kramer M, et al. Pulmonary venoocclusive disease: CT findings before and after single-lung transplantation. AJR Am J Roentgenol 1993;160: 759–760.

39. Storto ML, Kee ST, Golden JA, Webb WR. Hydrostatic pulmonary edema: high-resolution CT findings. AJR Am J Roentgenol 1995;165:817–820.

40. Swensen SJ, Tashjian JH, Myers JL, et al. Pulmonary venoocclusive disease: CT findings in eight patients. AJR Am J Roentgenol 1996;167:937–940.

41. Dufour B, Maitre S, Humbert M, Capron F, Simonneau G, Musset D. High-resolution CT of the chest in four patients with pulmonary capillary hemangiomatosis or pulmonary venoocclusive disease. AJR Am J Roentgenol 1998;171:1321–1324.

42. Ren H, Hruban RH, Kuhlman JE, et al. Computed tomography of inflation-fixed lungs: the beaded septum sign of pulmonary metastases. J Comput Assist Tomogr 1989;13:411–416.

43. Lynch DA, Hay T, Newell JD Jr, Divgi VD, Fan LL. Pediatric diffuse lung disease: diagnosis and classification using high-resolu-

tion CT. AJR Am J Roentgenol 1999;173:713–718.

44. Colby TV, Swensen SJ. Anatomic distribution and histopathologic patterns in diffuse lung disease: correlation with HRCT. J Thorac Imaging 1996;11:1–26.
45. Graham CM, Stern EJ, Finkbeiner WE, Webb WR. High-resolution CT appearance of diffuse alveolar septal amyloidosis. AJR Am J Roentgenol 1992;158:265–267.
46. Murch CR, Carr DH. Computed tomography appearances of pulmonary alveolar proteinosis. Clin Radiol 1989;40:240–243.
47. Godwin JD, Müller NL, Takasugi JE. Pulmonary alveolar proteinosis: CT findings. Radiology 1988;169:609–613.
48. Lee KN, Levin DL, Webb WR, Chen D, Storto ML, Golden JA. Pulmonary alveolar proteinosis: high-resolution CT, chest radiographic, and functional correlations. Chest 1997;111:989–995.
49. Murayama S, Murakami J, Yabuuchi H, Soeda H, Masuda K. "Crazy paving appearance" on high resolution CT in various diseases. J Comput Assist Tomogr 1999;23:749–752.
50. Johkoh T, Müller NL, Pickford HA, et al. Lymphocytic interstitial pneumonia: thin-section CT findings in 22 patients. Radiology 1999;212:567–572.
51. Ichikawa Y, Kinoshita M, Koga T, Oizumi K, Fujimoto K, Hayabuchi N. Lung cyst formation in lymphocytic interstitial pneumonia: CT features. J Comput Assist Tomogr 1994;18:745–748.
52. McGuinness G, Scholes JV, Jagirdar JS, et al. Unusual lymphoproliferative disorders in nine adults with HIV or AIDS: CT and pathologic findings. Radiology 1995;197:59–65.
53. Lynch DA, Webb WR, Gamsu G, Stulbarg M, Golden J. Computed tomography in pulmonary sarcoidosis. J Comput Assist Tomogr 1989;13:405–410.
54. Remy-Jardin M, Beuscart R, Sault MC, Marquette CH, Remy J. Subpleural micronodules in diffuse infiltrative lung diseases: evaluation with thin-section CT scans. Radiology 1990;177:133–139.
55. Müller NL, Kullnig P, Miller RR. The CT findings of pulmonary sarcoidosis: analysis of 25 patients. AJR Am J Roentgenol 1989;152:1179–1182.
56. Traill ZC, Maskell GF, Gleeson FV. High-resolution CT findings of pulmonary sarcoidosis. AJR Am J Roentgenol 1997;168:1557–1560.
57. Remy-Jardin M, Degreef JM, Beuscart R, Voisin C, Remy J. Coal worker's pneumoconiosis: CT assessment in exposed workers and correlation with radiographic findings. Radiology 1990;177:363–371.
58. Pickford HA, Swensen SJ, Utz JP. Thoracic cross-sectional imaging of amyloidosis. AJR Am J Roentgenol 1997;168:351–355.
59. Webb WR, Müller NL, Naidich DP. Standardized terms for high-resolution computed tomography of the lung: a proposed glossary. J Thorac Imaging 1993;8:167–185.
60. Akira M, Yamamoto S, Yokoyama K, et al. Asbestosis: high-resolution CT-pathologic correlation. Radiology 1990;176:389–394.
61. Nishimura K, Kitaichi M, Izumi T, Nagai S, Itoh H. Usual interstitial pneumonia: histologic correlation with high-resolution CT. Radiology 1992;182:337–342.
62. Primack SL, Hartman TE, Hansell DM, Müller NL. End-stage lung disease: CT findings in 61 patients. Radiology 1993;189:681–686.
63. Ujita M, Renzoni EA, Veeraraghavan S, Wells AU, Hansell DM. Organizing pneumonia: perilobular pattern at thin-section CT. Radiology 2004;232:757–761.
64. Gruden JF, Webb WR, Warnock M. Centrilobular opacities in the lung on high-resolution CT: diagnostic considerations and pathologic correlation. AJR Am J Roentgenol 1994;162:569–574.
65. Naidich DP, Zerhouni EA, Hutchins GM, Genieser NB, McCauley DI, Siegelman SS. Computed tomography of the pulmonary parenchyma. I. Distal air-space disease. J Thorac Imaging 1985;1:39–53.
66. Itoh H, Tokunaga S, Asamoto H, et al. Radiologic-pathologic correlations of small lung nodules with special reference to peribronchiolar nodules. AJR Am J Roentgenol 1978;130:223–231.
67. Im JG, Itoh H, Shim YS, et al. Pulmonary tuberculosis: CT findings—early active disease and sequential change with antituberculous therapy. Radiology 1993;186:653–660.
68. Lee KS, Kim YH, Kim WS, Hwang SH, Kim PN, Lee BH. Endobronchial tuberculosis: CT features. J Comput Assist Tomogr 1991;15:424–428.
69. Hartman TE, Swensen SJ, Williams DE. Mycobacterium avium-intracellulare complex: evaluation with CT. Radiology 1993;187:23–26.
70. Müller NL, Miller RR. Diseases of the bronchioles: CT and histopathologic findings. Radiology 1995;196:3–12.
71. Lynch DA, Rose CS, Way D, King TE. Hypersensitivity pneumonitis: sensitivity of high-resolution CT in a population-based study. AJR Am J Roentgenol 1992;159:469–472.
72. Akira M, Kita N, Higashihara T, Sakatani M, Kozuka T. Summer-type hypersensitivity pneumonitis: comparison of high-resolution CT and plain radiographic findings. AJR Am J Roentgenol 1992;158:1223–1228.
73. Remy-Jardin M, Remy J, Wallaert B, Müller NL. Subacute and chronic bird breeder hypersensitivity pneumonitis: sequential evaluation with CT and correlation with lung function tests and bronchoalveolar lavage. Radiology 1993;189:111–118.
74. Silver SF, Müller NL, Miller RR, Lefcoe MS. Hypersensitivity pneumonitis: evaluation with CT. Radiology 1989;173:441–445.
75. Akira M, Kitatani F, Lee YS, et al. Diffuse panbronchiolitis: evaluation with high-resolution CT. Radiology 1988;168:433–438.
76. Nishimura K, Kitaichi M, Izumi T, Itoh H. Diffuse panbronchiolitis: correlation of high-resolution CT and pathologic findings. Radiology 1992;184:779–785.
77. Akira M, Higashihara T, Sakatani M, Hara H. Diffuse panbronchiolitis: follow-up CT examination. Radiology 1993;189:559–562.
78. Ward S, Heyneman L, Lee MJ, Leung AN, Hansell DM, Müller NL. Accuracy of CT in the diagnosis of allergic bronchopulmonary aspergillosis in asthmatic patients. AJR Am J Roentgenol 1999;173:937–942.
79. Moore AD, Godwin JD, Müller NL, et al. Pulmonary histiocytosis X: comparison of radiographic and CT findings. Radiology 1989;172:249–254.
80. Müller NL, Staples CA, Miller RR. Bronchiolitis obliterans organizing pneumonia: CT features in 14 patients. AJR Am J Roentgenol 1990;154:983–987.
81. Leung AN, Miller RR, Müller NL. Parenchymal opacification in chronic infiltrative lung diseases: CT-pathologic correlation. Radiology 1993;188:209–214.
82. Collins J, Blankenbaker D, Stern EJ. CT patterns of bronchiolar disease: what is "tree-in-bud"? AJR Am J Roentgenol 1998;171:365–370.
83. Remy-Jardin M, Remy J, Gosselin B, Becette V, Edme JL. Lung parenchymal changes secondary to cigarette smoking: pathologic-CT correlations. Radiology 1993;186:643–651.
84. Gruden JF, Webb WR. CT findings in a proved case of respiratory bronchiolitis. AJR Am J Roentgenol 1993;161:44–46.
85. Holt RM, Schmidt RA, Godwin JD, Raghu

G. High resolution CT in respiratory bronchiolitis-associated interstitial lung disease. J Comput Assist Tomogr 1993;17:46–50.

86. Heyneman LE, Ward S, Lynch DA, Remy-Jardin M, Johkoh T, Müller NL. Respiratory bronchiolitis, respiratory bronchiolitis-associated interstitial lung disease, and desquamative interstitial pneumonia: different entities or part of the spectrum of the same disease process? AJR Am J Roentgenol 1999;173:1617–1622.

87. Akira M, Yokoyama K, Yamamoto S, et al. Early asbestosis: evaluation with high-resolution CT. Radiology 1991;178:409–416.

88. Howling SJ, Hansell DM, Wells AU, Nicholson AG, Flint JD, Müller NL. Follicular bronchiolitis: thin-section CT and histologic findings. Radiology 1999;212:637–642.

89. Remy-Jardin M, Remy J, Wallaert B, Bataille D, Hatron PY. Pulmonary involvement in progressive systemic sclerosis: sequential evaluation with CT, pulmonary function tests, and bronchoalveolar lavage. Radiology 1993;188:499–506.

90. Remy-Jardin M, Remy J, Cortet B, Mauri F, Delcambre B. Lung changes in rheumatoid arthritis: CT findings. Radiology 1994;193:375–382.

91. McGuinness G, Gruden JF, Bhalla M, Harkin TJ, Jagirdar JS, Naidich DP. AIDS-related airway disease. AJR Am J Roentgenol 1997;168:67–77.

92. Gruden JF, Webb WR, Sides DM. Adult-onset disseminated tracheobronchial papillomatosis: CT features. J Comput Assist Tomogr 1994;18:640–642.

93. Akira M, Atagi S, Kawahara M, Iuchi K, Johkoh T. High-resolution CT findings of diffuse bronchioloalveolar carcinoma in 38 patients. AJR Am J Roentgenol 1999;173:1623–1629.

94. Todo G, Herman PG. High-resolution computed tomography of the pig lung. Invest Radiol 1986;21:689–696.

95. Padley SP, Adler BD, Staples CA, Miller RR, Müller NL. Pulmonary talcosis: CT findings in three cases. Radiology 1993;186:125–127.

96. Akira M, Higashihara T, Yokoyama K, et al. Radiographic type p pneumoconiosis: high-resolution CT. Radiology 1989;171:117–123.

97. Primack SL, Miller RR, Müller NL. Diffuse pulmonary hemorrhage: clinical, pathologic, and imaging features. AJR Am J Roentgenol 1995;164:295–300.

98. Seely JM, Effmann EL, Müller NL. High-resolution CT of pediatric lung disease: imaging findings. AJR Am J Roentgenol 1997;168:1269–1275.

99. Johkoh T, Ikezoe J, Nagareda T, Kohno N, Takeuchi N, Kozuka T. Metastatic pulmonary calcification: early detection by high-resolution CT. J Comput Assist Tomogr 1993;17:471–473.

100. Hartman TE, Müller NL, Primack SL, et al. Metastatic pulmonary calcification in patients with hypercalcemia: findings on chest radiographs and CT scans. AJR Am J Roentgenol 1994;162:799–802.

101. Nolan RL, McAdams HP, Sporn TA, Roggli VL, Tapson VF, Goodman PC. Pulmonary cholesterol granulomas in patients with pulmonary artery hypertension: chest radiographic and CT findings. AJR Am J Roentgenol 1999;172:1317–1319.

102. Aquino SL, Gamsu G, Webb WR, Kee SL. Tree-in-bud pattern: frequency and significance on thin section CT. J Comput Assist Tomogr 1996;20:594–599.

103. Gruden JF, Webb WR. Identification and evaluation of centrilobular opacities on high-resolution CT. Semin Ultrasound CT MR 1995;16:435–449.

104. Lynch DA, Brasch RC, Hardy KA, Webb WR. Pediatric pulmonary disease: assessment with high-resolution ultrafast CT. Radiology 1990;176:243–248.

105. Franquet T, Gimenez A, Prats R, Rodriguez-Arias JM, Rodriguez C. Thrombotic microangiopathy of pulmonary tumors: a vascular cause of tree-in-bud pattern on CT. AJR Am J Roentgenol 2002;179:897–899.

106. Han D, Lee KS, Franquet T, et al. Thrombotic and nonthrombotic pulmonary arterial embolism: spectrum of imaging findings. RadioGraphics 2003;23:1521–1539.

107. Kim CK, Chung CY, Kim JS, Kim WS, Park Y, Koh YY. Late abnormal findings on high-resolution computed tomography after Mycoplasma pneumonia. Pediatrics 2000;105:372–378.

108. Reittner P, Müller NL, Heyneman L, et al. Mycoplasma pneumoniae pneumonia: radiographic and high-resolution CT features in 28 patients. AJR Am J Roentgenol 2000;174:37–41.

109. Wang BM, Stern EJ, Schmidt RA, Pierson DJ. Diagnosing pulmonary alveolar proteinosis: a review and an update. Chest 1997;111:460–466.

110. Holbert JM, Costello P, Li W, Hoffman RM, Rogers RM. CT features of pulmonary alveolar proteinosis. AJR Am J Roentgenol 2001;176:1287–1294.

111. Laurent F, Philippe JC, Vergier B, et al. Exogenous lipoid pneumonia: HRCT, MR, and pathologic findings. Eur Radiol 1999;9:1190–1196.

112. Lee KS, Müller NL, Hale V, Newell JD Jr, Lynch DA, Im JG. Lipoid pneumonia: CT findings. J Comput Assist Tomogr 1995;19:48–51.

113. Seo JB, Im JG, Kim WS, Seong CK, Song JW, Chung JH. Shark liver oil-induced lipoid pneumonia in pigs: correlation of thin-section CT and histopathologic findings. Radiology 1999;212:88–96.

114. Franquet T, Giménez A, Bordes R, Rodríguez-Arias JM, Castella J. The crazy-paving pattern in exogenous lipoid pneumonia: CT-pathologic correlation. AJR Am J Roentgenol 1998;170:315–317.

115. Cheon JE, Lee KS, Jung GS, Chung MH, Cho YD. Acute eosinophilic pneumonia: radiographic and CT findings in six patients. AJR Am J Roentgenol 1996;167:1195–1199.

116. Worthy SA, Müller NL, Hansell DM, Flower CD. Churg-Strauss syndrome: the spectrum of pulmonary CT findings in 17 patients. AJR Am J Roentgenol 1998;170:297–300.

117. Logan PM. Thoracic manifestations of external beam radiotherapy. AJR Am J Roentgenol 1998;171:569–577.

118. Tan RT, Kuzo RS. High-resolution CT findings of mucinous bronchioloalveolar carcinoma: a case of pseudopulmonary alveolar proteinosis. AJR Am J Roentgenol 1997;168:99–100.

119. Marti-Bonmati L, Ruiz PF, Catala F, Mata JM, Calonge E. CT findings in Swyer-James syndrome. Radiology 1989;172:477–480.

120. Webb WR. High-resolution computed tomography of obstructive lung disease. Radiol Clin North Am 1994;32:745–757.

121. Worthy SA, Park CS, Kim JS, Müller NL. Bronchiolitis obliterans after lung transplantation: high resolution CT findings in 15 patients. AJR Am J Roentgenol 1997;169:673–677.

122. Arakawa H, Webb WR. Expiratory high-resolution CT scan. Radiol Clin North Am 1998;36:189–209.

123. Webb WR. Radiology of obstructive pulmonary disease. AJR Am J Roentgenol 1997;169:637–647.

124. Martin KW, Sagel SS, Siegel BA. Mosaic oligemia simulating pulmonary infiltrates on CT. AJR Am J Roentgenol 1986;147:670–673.

125. King MA, Bergin CJ, Yeung DW, et al. Chronic pulmonary thromboembolism: de-

tection of regional hypoperfusion with CT. Radiology 1994;191:359–363.

126. Schwickert HC, Schweden F, Schild HH, et al. Pulmonary arteries and lung parenchyma in chronic pulmonary embolism: preoperative and postoperative CT findings. Radiology 1994;191:351–357.

127. Im JG, Kim SH, Chung MJ, Koo JM, Han MC. Lobular low attenuation of the lung parenchyma on CT: evaluation of forty-eight patients. J Comput Assist Tomogr 1996;20:756–762.

128. Arakawa H, Webb WR, McCowin M, Katsou G, Lee KN, Seitz RF. Inhomogeneous lung attenuation at thin-section CT: diagnostic value of expiratory scans. Radiology 1998;206:89–94.

129. Stern EJ, Webb WR, Golden JA, Gamsu G. Cystic lung disease associated with eosinophilic granuloma and tuberous sclerosis: air trapping at dynamic ultrafast high-resolution CT. Radiology 1992;182:325–329.

130. Stern EJ, Webb WR. Dynamic imaging of lung morphology with ultrafast high-resolution computed tomography. J Thorac Imaging 1993;8:273–282.

131. Webb WR, Stern EJ, Kanth N, Gamsu G. Dynamic pulmonary CT: findings in normal adult men. Radiology 1993;186:117–124.

132. Arakawa H, Kurihara Y, Sasaka K, Nakajima Y, Webb WR. Air trapping on CT of patients with pulmonary embolism. AJR Am J Roentgenol 2002;178:1201–1207.

133. Chung MH, Edinburgh KJ, Webb EM, McCowin M, Webb WR. Mixed infiltrative and obstructive disease on high-resolution CT: differential diagnosis and functional correlates in a consecutive series. J Thorac Imaging 2001;16:69–75.